Agren, D., Stehr, M., Berthold, C.L., Kapoor, S., Oehlmann, W., Singh, M., Schneider, G.
Three-Dimensional Structures of Apo- and Holo-l-Alanine Dehydrogenase from Mycobacterium tuberculosis Reveal Conformational Changes upon Coenzyme Binding
(2008) Journal of Molecular Biology, 377 (4), pp. 1161-1173.

Three-dimensional structures of apo- and holo L-alanine dehydrogenase from *Mycobacterium tuberculosis* reveal conformational changes upon coenzyme binding

Daniel Ågren[1], Matthias Stehr[3], Catrine L. Berthold[1], Shobhna Kapoor[3], Wulf Oehlmann[2], Mahavir Singh[2, 3] and Gunter Schneider[1*]

1. Department of Medical Biochemistry and Biophysics, Karolinska Institutet, S-171 77 Stockholm, Sweden
2. LIONEX GmbH, Inhoffenstrasse 7, D-38124 Braunschweig, Germany
3. Helmholtz Center for Infection Research, Inhoffenstrasse 7, D-38124 Braunschweig, Germany

*: send correspondence to Gunter.Schneider@ki.se

Running title: Crystal structures of mycobacterial alanine dehydrogenase

Abstract

L-alanine dehydrogenase from *Mycobacterium tuberculosis* catalyzes the NADH dependent reversible conversion of pyruvate and ammonia to L-alanine. Expression of the gene coding for this enzyme is up-regulated in the persistent phase of the organism, and alanine dehydrogenase is therefore a potential target for pathogen control by antibacterial compounds. We have determined the crystal structures of the apo- and holoforms of the enzyme to 2.3 and 2.0 Å resolution, respectively. The enzyme forms a hexamer of identical subunits, with the NAD binding domains building up the core of the molecule, and the substrate binding domains located at the apical positions of the hexamer. Coenzyme binding stabilizes a closed conformation where the substrate binding domains are rotated by about 16° towards the dinucleotide binding domains, compared to the open structure of the apo-enzyme. In the structure of the abortive ternary complex with NAD+ and pyruvate, the substrates are suitably positioned for hydride transfer between the nicotinamide ring and the C2 carbon atom of the substrate. The approach of the nucleophiles water and ammonia to pyruvate or the reaction intermediate iminopyruvate, respectively, is however only possible through conformational changes that make the substrate binding site more accessible. The crystal structures identified the conserved active site residues His96 and Asp270 as potential acid/base catalysts in the reaction. Amino acid replacements of these residues by site-directed mutagenesis led to inactive mutants, further emphasizing their essential roles in the enzymatic reaction mechanism.

Keywords: enzyme mechanism, protein structure, X-ray crystallography, ternary complex, persistent tuberculosis

Abbreviations

L-AlaDH, L-alanine dehydrogenase; *Mt*AlaDH, L-alanine dehydrogenase from *Mycobacterium tuberculosis*; *Pl*AlaDH, L-alanine dehydrogenase from *Phormidium lapideum*; r.m.s.d, root-mean-square deviation;

Introduction

In view of the annual death toll of approximately 2 million individuals due to infection by *Mycobacterium tuberculosis* the emergence of multi-drug resistant and extensively drug resistant strains of *Mycobacterium tuberculosis* poses a major threat to human health worldwide (WHO homepage: http://www.who.int). Treatment of this disease is further complicated by the ability of *M. tuberculosis* to persist in the lungs of infected individuals for decades by switching to a dormant or latent phase[1], which also induces tolerance to current antibiotics[2,3]. About one-third of the world's population is infected with persistent mycobacteria providing an enormous potential reservoir for further spread of this disease. Dormancy has been associated with non-replicating or very slow growth of *M. tuberculosis* that resides in granulomas, a heterogeneous assembly of macrophages, in the lungs of infected individuals. It is generally assumed that the microenvironment in the granulomas is characterized by hypoxia, nutrient starvation and reactive oxygen and nitrogen species[4-6].

Several experimental *in vitro* models for the dormant phase of the bacilli have been developed, albeit their relevance to human latent infection is still a matter of debate. A widely used *in vitro* approach to mimic dormancy is based on culture of *M. tuberculosis* under microaerophilic/anaerobic conditions[7]. Other models of dormancy utilize nutrient starvation[8] or treatment by nitric oxide[9]. Drug-induced persistence has been studied *in vitro* using stationary *M. tuberculosis* grown under microaerophilic conditions treated with rifampicin or *in vivo* by pyrazinamide-induced persistent bacteria in mice[10]. These model systems have been employed to study the metabolic state of the bacteria in the dormant phase. Comparison of gene-expression profiles and proteome analyses of active versus non-replicating bacteria have identified a number of genes that are up-regulated in persistent *M. tuberculosis*[8,11-16]. One of these genes, Rv2780, found to be over-expressed under hypoxic[14,15] and nutrient starvation[8] regimes encodes L-alanine dehydrogenase (L-AlaDH). Increased levels of this enzyme have been linked to the generation of alanine for peptidoglycan biosynthesis[15,17] and the maintenance of the NAD+ pool under conditions when the terminal electron acceptor oxygen becomes limiting[8,15,18].

L-AlaDH catalyzes the NADH-dependent conversion of pyruvate and ammonia to L-alanine (Figure 1), and is involved in microbial carbon and nitrogen metabolism. The mycobacterial enzyme is secreted into the culture medium, and is identical to the 40 kDa antigen that has been identified in culture filtrates of *M. tuberculosis*[19]. In solution the enzyme forms a

hexamer of six identical subunits (predicted molecular mass 38988 Da per subunit) [20], as observed for most L-alanine dehydrogenases from other species, for instance *Phormidium lapideum*[21], *Streptomyces phaeochromogenes*[22] and *Bacillus subtilis*[23]. The hexameric molecule of L-AlaDH from *Phormidium lapideum* shows 32 point group symmetry, and is best described as a trimer of dimers[24].

Kinetic and mechanistic studies of L-alanine dehydrogenases from several species[17,25-28] showed that the enzyme follows a predominantly ordered mechanism, with NAD+ and NADH binding occurring first in the oxidative deamination and reductive amination direction, respectively. The enzymatic mechanism most likely proceeds through imino acid and carbinolamine intermediates[27]. Crystal structures of binary complexes of L-AlaDH from *Phormidium lapideum* have identified the binding sites of NAD+ and pyruvate[24]. The nicotinamide ring in the L-AlaDH-NAD+ binary complex, obtained by soaking crystals of the apo-enzyme with the nucleotide diphosphate, is however not in a position suitable for hydride transfer from the nicotinamide group to pyruvate. It has therefore been questioned whether this complex represents the catalytically active species[24].

Here we report the three-dimensional structures of apo- and holo-L-AlaDH from *M. tuberculosis.* The structures reveal a conformational transition in the form of a 16° rotation upon binding of the dinucleotide, from an "open" to a "closed" conformation. This conformational change ensures proper orientation of the substrates for hydride transfer to occur and excludes bulk water from the active site. The crystal structures and complementary site-directed mutagenesis studies support a mechanistic model where conformational changes are required to allow access of water and ammonia to the active site, and where the active site residues His96 and Asp270 participate in proton transfer steps during catalysis.

Results and discussion

Subunit structure

The subunit of L-AlaDH is built up of two distinct domains, the substrate binding domain (residues 1-128 and 309-371) and the NAD-binding domain (residues 129-308), connected by two α helices (Figure 2a). Both domains contain variants of the classical dinucleotide binding fold common to NAD dependent dehydrogenases[29]. The NAD binding domain is characterized by a central seven-stranded mixed β-sheet flanked by α-helices, with one of the

edge strands being anti-parallel to the rest of the sheet. The core of the substrate binding domain folds into an eight-stranded β-sheet, containing a six-stranded parallel Rossmann fold, extended by a β-hairpin motif at one side. The two domains are structurally similar to each other (r.m.s.d 2.4 Å, for 82 equivalent Cα atoms), although there is no detectable sequence similarity. The domains are packed such that the C-terminal ends of the β-sheets face each other across a cleft that contains the active site (Figure 2a). Residues from both domains thus contribute to active site topology and also provide catalytic groups.

Quaternary structure

Gel filtration experiments suggested that *Mt*AlaDH forms a hexamer in solution. The structure of *Mt*AlaDH has been determined in three different crystal forms (Table 1), which all contain a hexameric molecule, consistent with the solution data. In crystal form $P2_12_12$ the asymmetric unit contains a hexamer of 32 symmetry, with a three-fold non-crystallographic axis coinciding with the molecular three-fold axis. In space groups P321 and $P2_13$, which both contain a dimer in the asymmetric unit the hexamer is generated by crystallographic three-fold axes. The quaternary structure is best described as a trimer of dimers (Figure 2b & c), with the core of the molecule formed by the six NAD binding domains, and the substrate binding domains located at the apical positions of the hexamer (Figure 2c). This packing of the subunits in the hexamer generates two major interfaces, the 'dimer' interface between two subunits from the upper and lower layers of the hexamer, and the 'trimer' interface between adjacent 'dimers' in the hexamer.

The 'dimer interface' formed by the NAD domains (Figure 2b) includes the most extensive interactions and is responsible for the AlaDH dimer being the building block of the hexamer. This interface region is located far from the active site (Figure 2b) and buries a surface of more than 1700 $Å^2$. Most of the interactions between residues involved in this interface are hydrophobic, but include one salt bridge and ten hydrogen bonds.

The 'trimer interface' is smaller and buries about 1100 $Å^2$, with the majority of the interactions almost exclusively between the NAD domains from adjacent dimers. These interactions involve two salt bridges (Asp208-Arg139/Arg185 and Arg205-Glu135), twelve hydrogen bonds and hydrophobic interactions. The trimer interface also includes interactions through residues from loop 163-166 and β-strand 215-219 with their symmetry related

counterparts from an adjacent NAD domain. The substrate-binding domain contributes much less to the trimer interface and interacts exclusively with the NAD domain of the adjacent dimer through hydrophobic interactions between residues Pro20 and Ala21 that pack against the side chain of Tyr223. There are no direct interactions between adjacent substrate binding domains in the hexamer.

The structure of holo-MtAlaDH reveals a conformational transition upon dinucleotide binding

*Mt*AlaDH binds NADH rather strongly, with a K_d of 8.2 μM determined from the concentration dependence of the change in fluorescence emission at 390 nm of NADH upon binding to the enzyme (Figure 3a). A similar value, 10.7 μM, is obtained for the K_m of NADH in the reductive amination reaction (Figure 3b). Crystallisation of *Mt*AlaDH in the presence of saturating concentrations of NADH resulted in a crystal form different from that of the apo-enzyme, space group $P2_13$, and the structure of the holo-enzyme was therefore determined by molecular replacement to 2.0 Å resolution (Figure 3c, Table 1).

The major structural difference between apo- and holo-*Mt*AlaDH is a shift in the relative orientation of the two domains upon binding of NADH (Figure 4). This conformational change can be described by a rigid-body rotation of the substrate-binding domain by approximately 16° around an arbitrary axis towards the NAD domain, resulting in maximum displacements of main chain carbon atoms in loop 357 -360 by 11 Å from their position in the apo-enzyme. Two helices, α5 (residues 126-133) and η7 (residues 304-320), act as hinge region for the domain movement, determined by the program Dyndom[30]. The fact that the domain movement can be described as a closure of the substrate binding domain towards the NAD domain and not *vice versa* is suggested by the analysis of the hexamer packing in apo- and holo-*Mt*AlaDH. The core of the hexamer, and the composition of the interfaces involving the NAD domains is identical in both molecules, indicating that the packing and orientation of the NAD domains in the hexamer is not changed upon binding of NADH. The domain contacts involving the substrate binding domains are however different in the two structures, resulting in a moderate decrease of the size of the trimer interface from 1100 Å to 970 Å and loss of the interaction between Tyr223 of the NAD domain and the loop from the substrate-binding domain of the neighbouring dimer in the holoenzyme. Several segemtns of the polypeptide chain that were without interpretable electron density in the apo-enyzme are well

ordered in the structure of the binary complex. These regions include two loop regions (residues 241-253 and 267-293) that participate in the binding of NADH.

The shift of the substrate binding domain towards the NAD domain in the holo-enzyme results overall in a more closed conformation of the active site, and in particular in changes in the position of several putative active site residues, which are closer to NADH in holo-*Mt*AlaDH. This suggests that the closed conformation reflects a catalytically relevant state of the enzyme whereas in the open form the substrates and catalytic groups are not properly positioned for catalysis. The crystal structure of apo-*Mt*AlaDH is similar to the structures of AlaDH from *Phormidium lapideum*[24] and *Thermos thermophilus* AlaDH (RIKEN Structural Genomics Initiative, PDB accession code 2eez). Superposition results in rms deviations of 1.0 Å (334 equivalent Cα atoms) for *Pl*AlaDH (pdb code: 1pjb) and 0.9 Å (337 equivalent Cα atoms) for *Tt*AlaDH (pdb code: 2EEZ). These crystal structures of the homologues represent the open form of the enzyme and thus do not reveal all features of the active enzyme.

NAD binding

In the electron density maps of the holo-enzyme, well-defined electron density at the expected dinucleotide binding site was observed that allowed a straightforward fit of NADH to the electron density (Figure 3c). The dinucleotide is bound in an extended conformation, with the ribose sugar rings in C2' endo conformation. As in other enzymes of the NAD dehydrogenase family, the dinucleotide is bound to *Mt*AlaDH at the C-terminal end of the β-sheet, with the diphosphate group positioned at the cross-over connection between strands β3 and β4[31]. The adenine ring of NADH interacts with the enzyme mainly via hydrophobic interactions with residues Ile199, Val239, Leu240 and Leu249. Similar to *Pl*AlaDH there are hydrogen bonds between the 2´- and 3´-hydroxyl groups of the adenine ribose and a conserved acidic residue, Asp198. An additional hydrogen bond is formed between the 2´-hydroxyl of NAD and the ε-nitrogen atom of Lys-203. The pyrophosphate moiety makes a number of contacts through hydrogen bonds to main chain atoms of the loop 178-179 and to the side chain of Ser134. The hydroxyl groups of the nicotinamide ribose form a bifurcated hydrogen bond to the carboxyl group of Asp270. The nicotinamide ring is bound in a pocket formed by residues Met133, Ser134, Ala137, Ile267, Asp270 and Met301. Hydrogen bonds are formed from backbone atoms of Ile267, Val298 and Met301 to the oxygen and nitrogen atoms of the carboxamide group of the nicotinamide ring which position this group such that the 4-pro-R hydrogen

points towards the active site pocket. This binding mode of the nicotinamide ring is consistent with the classification of AlaDH as a class A (pro-R) NAD-dependent dehydrogenase[31].

Crystallisation of *Mt*AlaDH at lower concentrations of the dinucleotide, 0.5 – 1 mM, resulted in a hybrid hexamer, where only the subunits from one dimer were in the closed conformation, and the four remaining subunits remained in the open conformation. While the subunits in the closed conformation contained NADH at full occupancies, the remaining four subunits did not contain NADH, or only at low occupancies. However, soaking of these crystals (space group $P2_12_12$) in 10 mM NADH led to full occupancies of all six binding sites, without triggering the conformational change in the open subunits, most likely due to crystal packing interactions. The interactions of NADH with *Mt*AlaDH are identical in the open and closed conformation. The position of the dinucleotide bound to the open form of *Mt*AlaDH is similar to that seen in the complex of *Pl*AlaDH with NAD^+ [24]. There are however differences in interactions of the dinucleotide with the enzyme. The most significant is the lack of the bifurcal hydrogen bond of the side chain of Asp270 to the nicotinamide ribose in *Pl*AlaDH. The side chain of the corresponding aspartic acid residue in *Pl*AlaDH (Asp269) points away from the ribose moiety into the solvent.

Structure of a ternary complex of MtAlaDH with NAD+ and pyruvate

In attempts to obtain structural information on ternary complexes of the enzyme with substrates, co-crystallisation experiments of *Mt*AlaDH as abortive ternary complexes with NADH/alanine and NAD+/pyruvate/NH_3 were carried out. While the combination enzyme-NADH-alanine was unsuccessful, crystals obtained in the presence of 10 mM NAD+, 10 mM NH_3 and 30 mM pyruvate were similar in shape to those of the holo-enzyme, but did not diffract X-rays. However, *Mt*AlaDH co-crystallized with lower concentrations of the substrates (0.5 mM NAD+, 10 mM NH_3, and 5 mM pyruvate) gave orthorhombic crystals (space group $P2_12_12$) that diffracted to 2 Å resolution. These crystals also contain a mixed hexamer with two closed and four open subunits in the asymmetric unit, as described above, and only the subunits in the closed conformation contain bound ligands.

The electron density for the bound NAD+ is well defined. The binding mode of NAD+ in the ternary complex is identical to that observed in the holo-enzyme obtained with NADH and all enzyme-dinucleotide interactions are maintained. Additional difference electron density in the active site pockets indicated the presence of a bound ligand that was modelled as formate, the

precipitating agent used in crystallisation (Figure 5). Residual difference electron density maps after refinement however suggested that this binding site is in part occupied by a larger molecule (Figure 5a). Modelling of this difference density by pyruvate and subsequent refinement revealed that the occupancy is lower than 1.0 (Figure 5b), and the crystals contain a mixture of the enzyme/NAD+/pyruvate and enzyme/NAD+/formate complexes.

The carboxyl group of pyruvate binds at the bottom of the cleft between the two domains, and is tightly anchored to the enzyme through hydrogen bonds and charge interactions via its oxygen atoms to the side chains of Arg15 and Lys75 (Figure 5). Lys75 is within hydrogen-bonding distance to the carbonyl oxygen of pyruvate and the side chain of His96 also forms a hydrogen bond to the pyruvate carbonyl oxygen atom. Additional non-polar interactions are formed to residues Phe94, Leu130, Met133 and Ala299. Most of these enzyme-substrate interactions are also found in the open form of the enzyme[24], but there are two significant differences. As a result of the rigid body movement of the substrate binding domain towards the NAD domain pyruvate is located closer to the coenzyme, with a distance of 3 Å between the C4 carbon atom of the nicotinamide ring and the C2 carbon atom of pyruvate (Figure 6). The latter is stacked against the nicotinamide ring of NAD, in a position suitable for hydride transfer. In addition the side chain of Asp270 is within hydrogen bonding distance to the carbonyl oxygen atom of pyruvate (Figure 5 & 6).

Site-directed mutagenesis

The crystal structures described here identified the conserved residues His96 and Asp270 as putative catalytic groups and the function of these groups in catalysis was therefore probed by site-directed mutagenesis (Table 2). Replacement of Asp270 by alanine or asparagine, respectively, resulted in completely inactive mutants that did not allow a more detailed kinetic analysis. The comparison of the crystal structures of the Asp270Asn mutant and wild-type *Mt*AlaDH showed that the bifurcated hydrogen bond between Asp270 and the ribose of NAD is replaced by a single hydrogen bond. There are no other differences in the positions of active site residues or the bound co-substrate NADH, thus excluding structural defects as the major cause for the catalytic deficiency of this mutant. The amino acid replacement at position His96 also resulted in an enzyme variant with no detectable catalytic activity.

Implications for the catalytic mechanism

Based on a detailed kinetic analysis of AlaDH from *Bacilllus subtilis* it was proposed that the enzymatic reaction follows a predominantly ordered mechanism and proceeds through iminopyruvate and carbinolamine intermediates[26,27]. The first step in the reductive amination reaction (Figure 1) is the binding of NADH, which as shown in this study stabilizes a closed conformation where the substrate-binding domain moved towards the NADH binding domain. In the ternary complex pyruvate is anchored to the active site through interactions with the side chains of Arg15 and Lys75. The hydrogen bond to Lys75 may further polarise the carbonyl oxygen atom thus facilitating nucleophilic attack of ammonia on the carbonyl carbon atom resulting in a carbinolamine intermediate. Protonation of the hydroxyl group and subsequent release of water yields the protonated iminopyruvate, which is reduced to L-alanine. In the ternary complex *Mt*AlaDH-NAD+-pyruvate (Figures 5 & 6) the distance between the C4 of the nicotinamide ring and the Cα carbon atom of pyruvate, and by analogy of iminopyruvate, is 3 Å, suitable for direct hydride transfer. The closed conformation further ensures a hydrophobic environment that favours hydride transfer reactions. We therefore conclude that the structure of the enzyme observed in the ternary complex represents the conformation relevant for the hydride transfer step in the mechanism. It is particularly noteworthy that pyruvate is packed tightly against the nicotinamide ring, and is inaccessible to the solvent. There are no bound water molecules observed in the immediate vicinity of the substrate that might indicate binding sites for the nucleophiles in the reaction, water and ammonia.

Cleland and colleagues[27] suggested that the attack on the iminopyruvate by the water molecule (i.e. direction of oxidative deamination) occurs from the same site as the nicotinamide ring, i.e. on the *re* face of pyruvate, whereas the attack of ammonia onto pyruvate (i.e. in the direction of reductive amination) occurs from the opposite face. Since the stereochemistry of the resulting carbinolamine intermediate is not yet unambiguously established experimentally, the direction of attack of the two nucleophiles could be reversed, resulting in a carbinolamine with L-hydroxy and D-amino groups. The tight packing of pyruvate (and by analogy iminopyruvate) against the nicotinamide ring in the model of the abortive ternary complex enzyme-NAD+-pyruvate is however not consistent with an attack by the water molecule (or ammonia for that matter) on the *re* face of the intermediate. In order to make pyruvate and iminopyruvate accessible, the enzyme must adopt a more open

conformation at these stages of catalysis in order to allow approach of water and ammonia from the bulk solution, as has been suggested for glutamate dehydrogenase[33].

The extent of the required conformational changes is not necessarily very large. For instance, the *si* face of pyruvate can be made accessible through a rearrangement of the side chain of Lys75, which in the closed structure blocks access to pyruvate. A movement towards the adjacent side chain of Glu76 opens a narrow channel from the bulk solution to the bound pyruvate that would allow diffusion of ammonia into the active site (figure 7). It is however not as obvious how the *re* face of pyruvate could be made accessible other than through a partial or complete domain rotation towards the conformation seen in the apo-enzyme. Factors that might trigger these and other conformational transitions could be the displacement of the positive charge from NAD+ via the iminonitrogen atom to the participating enzymic residue(s) (Figure 1) during catalysis, as well as the changes in hybridisation of the Cα carbon of L-alanine from sp^3 to sp^2. A more detailed description of the nature of these structural re-arrangements however has to await further studies of ternary and quaternary complexes of holo-*Mt*AlaDH with L-alanine and pyruvate/NH_3.

Several catalytic steps involve proton transfer reactions (Figure 1). Two conserved residues, His96 and Asp270, are suitably positioned at a distance of 3 Å to the pyruvate carbonyl oxygen atom, and therefore are potential acid/base catalysts in the reaction. To further investigate the role of these residues in catalysis Asp270 was exchanged to alanine and asparagine, and His96 to alanine, respectively, by site-directed mutagenesis. Amino acid replacements at these positions led to completely inactive mutant enzymes, and the mutagenesis data thus support critical roles of these conserved residues, possibly as acid/bases in catalysis by *Mt*AlaDH. It is at present, however, not yet clear whether these two residues act in concert (i.e. as a proton relay system) for both proton transfer steps, or if they participate individually at different stages of catalysis, for instance that Asp270 protonates the water molecule after nucleophilic attack and His96 abstracts a proton from the amino group of the carbinolamine or *vice versa* (Figure 1).

In conclusion, the structure analysis of apo- and holo-alanine dehydrogenase from *Mt tuberculosis* has revealed two conformations of the enzyme. The conformation observed in the presence of the coenzymes NAD+ and NADH, respectively, is characterized by (i) domain closure leading to an active site inaccessible to solvent molecules and favourable for hydride

transfer and (ii) completion of the active site by approach of conserved residues that interact with the substrate and participate in catalysis. Furthermore, the closed conformation ensures proper orientation of the nicotinamide ring and the substrate suitable for hydride transfer. Other steps of the catalytic mechanisms require approach of small nucleophiles such as water and ammonia to the reaction intermediates, which is only possible through conformational changes that make the substrate binding site more accessible.

Methods

Protein production: Wild-type *Mt*AlaDH was produced in *E. coli* BL21(DE3) containing the Mt *ald* gene in pET26 (Novagen, UK). The recombinant strain was grown at 30 °C in LB-medium containing 50 µg/mL kanamycin. Induction was performed in mid-log-phase by addition of 1.0 mM IPTG and bacterial cells were harvested 3 hours after induction. The cells were disrupted by sonication, and the crude extract was centrifuged at 20.000 x g for 15 min. The resulting supernatant was filtered and applied to Ni-NTA resin. Recombinant protein was eluted from the column using an imidazole gradient. The highly purified protein (more than 98% purity as judged by stained SDS-PAGE gels) was stored in 10 mM ammonium bicarbonate buffer, pH 7.7 at 4 °C.

Site-directed mutagenesis: For site directed mutagenesis, two complementary primers containing the desired mutation (D270A: 5′-ATAGCCATCGCTCAGGGCGGCT-3′ and 5′-AGCCGCCCTGAGCGATGGCTAT-3′; D270N: 5′-ATAGCCATCAATCAGGGCGGCT-3′ and 5′-AGCCGCCCTGATTGATGGCTAT-3′; H96A: 5′-ACGTTCTTGGCTTTGGCCGCGT-3′ and 5′-ACGCGGCCAAAGCCAAGAACGT-3′) together with cloning primers specific to the 5′- and 3′-end of *ald* (forward: 5′-GGGCCCCATATGCGCGTCGGTATTCC-3′; reverse: 5′-GGGCCCAAGCTTCAATGGTGATGGTGATGGTGGGCCAGCACGCTGGCGG-3′), respectively, were used for amplification of the two fragments. The template for construction of the mutants was the *ald* gene without the *Nde*I restriction site. The purified PCR-products were used in a second round of PCR of five cycles and the resulting two fragments were combined and re-amplified in order to obtain the entire mutated gene. Mutants were verified by DNA analysis. Mutated *ald* was inserted into *Nde*I- and *Hin*dIII-sites of the expression vector pET26 (Novagen, UK) and the *Mt*AlaDH mutants were produced in *E. coli* BL21(DE3) and purified as described above.

Enzyme assays: Specific activities of recombinant *Mt*AlaDH were determined using the assay previously described[17]. For the determination of the Km value of NADH in the reductive amination direction, *Mt*AlaD (0.17 µg/ml) was assayed at 298 K in 0.1 M NH_4^+/NH_3 buffer, pH 7.4 with 20 mM pyruvate in a final reaction volume of 1 ml. The reaction was started by the addition of 25 µl NADH of appropriate concentrations (final concentration range 5 µM to 320 µM) to the reaction mixture. The rate of the reaction was followed at a wavelength of 340 nm using a Jasco V-650 spectrophotometer. The photometric determination of the kinetic parameters for L-alanine and pyruvate, respectively, was carried out as follows. For the oxidative deamination the reaction mixture consisted of 25 nM *Mt*AlaDH, 125 mM glycine/KOH (pH 10.2), 1.25 mM NAD+ and variable concentrations of L-alanine (0.1 – 60 mM). For the reductive amination the assay consisted of 25 nM *Mt*AlaDH, 1.0 M NH_4Cl/NH_3, pH 7.4, 0.25 mM NADH and variable concentrations of pyruvate (3.0 - 400 µM). All measurements were performed at 340 nm with a SAFAS UV mc2 spectrophotometer. The kinetic parameters were derived using Prism 5 (GraphPad Software, San Diego, USA).

Binding assay of NADH: The binding constant of NADH to *Mt*AlaDH was determined by following the change in fluorescence emission at 390 nm as a function of NADH concentration. The data points were fitted to the equation $\Delta A_{390}=\Delta A_{390,\ max}$ (NADH)/(K_d + (NADH)) [34]. The fluorescence assays were carried out using a Shimadzu RF-510LC fluorescence spectrophotometer. NADH was excited at 331 nm, and the emission at 390 nm was measured to monitor NADH binding. Measurements were performed with 15 µM *Mt*AlaDH in 20 mM NH_4Cl/NH_3, pH 7.4 with stepwise addition of NADH in the concentration range 1-30 µM.

Crystallization: Crystallization experiments were performed using the vapour-diffusion technique. A protein solution of 6.8 mg/ml *Mt*AlaDH in 10 mM ammonium bicarbonate buffer, pH 8.9 was used throughout the crystallization experiments. Initial screening using commercial sparse matrix crystallization screens gave several hits, which could then be further optimized in 24-well hanging drop plates. Typically, 2 µl aliquots of the protein solution were mixed with 2 µl reservoir solution and set up against 1ml well solution.

Crystals of apo-*Mt*AlaDH were grown using 0.4 M ammonium hydrogenphosphate as reservoir solution at 293 K. For co-crystallisation of holo-*Mt*AlaDH, an enzyme solution

containing 10 mM NADH was equilibrated at 277 K for 24 h with a well solution containing 23 % PEG 3350, 0.2 M sodium acetate and 0.1 M BisTris propane pH 8.2. Streak seeding resulted in well-diffracting crystals of the holoenzyme. A second crystal form of *Mt*AlaDH in the presence of NADH (1 mM) was obtained at 277 K after 2-3 days equilibration against a well solution containing 13% ethanol, 0.2 M $MgCl_2$ and 0.1 M Hepes buffer pH 7.4. These crystals were also used for soaking experiments at higher NADH concentrations (10 mM). A putative ternary complex of *Mt*AlaDH, pyruvate and NAD+ was obtained at 293 K by co-crystallisation of an enzyme solution containing 0.5 mM NAD^+ and 5 mM pyruvate using a well solution containing 0.1 M Hepes buffer pH 7.2 and 0.45 M $Mg(HCO_2)_2$. Co-crystallisation of the mutant D270N *Mt*AlaDH with NADH was carried out using the same protocol as for wild-type holo-*Mt*AlaDH.

All crystals were flash frozen in liquid nitrogen after transfer for a few seconds into mother liquor containing 30% glycerol. For the soaking experiments the crystals were left for 10 min in mother liquid containing 30% glycerol and 10 mM NADH before flash-freezing.

Data collection and structure determination: All data were collected in a nitrogen stream at 110 K using synchrotron radiation at MaxLab, Lund, Sweden and at the ESRF, Grenoble, France. Images were processed with the program MOSFLM and scaled using the program SCALA from the CCP4 suite[35].

The best crystals of the apoenzyme diffracted to 2.3 Å resolution. Initially, the space group P622 was assigned, but inspection of the intensity distribution clearly indicated merohedral twinning. The CCP4 programs Truncate[36] and Detwin[37] in combination with analysis of self-rotation function plots calculated with Molrep[38] were used to further analyze crystal twinning. The 'Merohedral Crystal Twinning Server' [39] was used for the calculation of the twin fraction. The twin tests suggested hemihedral twinning, with the true space group being P321 and an estimated twin fraction of 0.3. Molecular replacement was performed using the twinned data and the programm Phaser[40] with *Pl*AlaDH (Pdb code: 1PJC) as search model. Two molecules per asymmetric unit were found. The structure of apo *Mt*AlaDH was refined to 2.3 Å with a fixed twin fraction of 0.3 using the protocol for data with hemihedral twinning in CNS[41]. A test set was excluded to monitor the R_{free}. Care was taken not to bias the refinement and twin-related reflections were kept together in either the test or work set. Refinement with simulated annealing, individual B-factors, and energy minimization procedures was alternated with

model building in Coot[42]. Initially, non-crystallographic symmetry restraints were applied, but were removed in later stages of the refinement. Water molecules were added automatically in Coot and inspected manually. Electron density for several disordered loop regions (subunit A: residues 240-258, 269-293, 298-300; subunit B: residues 240-254, 268-293, 297-300) was missing or very weak and these residues were therefore not included in the final model. Details of model statistics after refinement are given in table 1.

Crystals of *Mt*AlaDH obtained in the presence of pyruvate and NAD^+ belong to the space group $P2_12_12$, with a hexamer in the asymmetric unit. The structure was determined by molecular replacement with the program Molrep[38] using one subunit of the refined apo-enzyme as search model. In the first run, four of the subunits were positioned. The remaining NAD binding domains were placed in a second run using only this domain as a search model. The substrate domains of these two subunits were then manually placed in the electron density, followed by rigid body refinement with the individual domains as separate rigid bodies. After rigid body refinement NADH was manually fitted in the residual electron density using the program Coot[42].

The crystals obtained in the presence of 10 mM NADH belong to the cubic space group $P2_13$ with one dimer in the asymmetric unit. The structure was phased using the refined closed monomer of *Mt*AlaDH (NADH excluded from the model) as search model in Molrep[38].

Refinement of the structures of the binary and ternary complexes followed similar protocols. Rounds of refinement with REFMAC5[43] were interspersed with manual model building in Coot. Atomic displacement parameters were refined in REFMAC by the TLS method[44], with each domain of the monomers treated as a single TLS group. Bound ligands were placed manually in the electron density and water molecules were added automatically and inspected manually. The NAD molecules bound to the subunits in the closed conformation of the enzyme showed full occupancies, while in some of the subunits in the open conformation NAD was modelled at occupancies of 0.5.

Refinement of the *Mt*AlaDH D270N mutant holo-enzyme was performed in a similar way as for the wild-type protein. The structure was determined using the closed holo-enzyme as a search model in Molrep[38], followed by rounds of refinement with REFMAC5[43] which were interspersed with manual model building in Coot[42].

The final models were validated with PROCHECK[45]. Structural comparisons were carried out using SSM[46]. All figures visualising protein models were prepared using PyMOL (www.pymol.org). The atomic coordinates and observed structure factor amplitudes of *Mt*AlaDH have been deposited to the Protein Data Bank, accession codes 2VHY (apoenzyme), 2VHZ (holoenzyme), 2VHW (holohybrid-enzyme), 2VHX (ternary complex with pyruvate and NAD+) and 2VHV (holo-Asp270Asn mutant).

Acknowledgements

We gratefully acknowledge access to synchrotron radiation at the ESRF, Grenoble, France and MAX laboratory, Lund University, Sweden. We also thank Ralf Morgenstern, Karolinska Institutet, for access to a spectrofluorometer. This work was supported by the European Commission; contract LSHP-CT-2005-018729.

References

1. Bloom, B. R. & McKinney, J. D. (1999). The death and resurrection of tuberculosis. *Nat Med* **5**, 872-874.
2. Wayne, LG & Sramek, HA. (1994) Metronidazole is bactericidal to dormant cells of Mycobacterium tuberculosis. *Antimicrob Agents Chemother.* **38**, 2054-2058.
3. Wallis, R. S., Patil, S., Cheon, S. H., Edmonds, K., Phillips, M., Perkins, M. D., Joloba, M., Namale, A., Johnson, J. L., Teixeira, L., Dietze, R., Siddiqi, S., Mugerwa, R. D., Eisenach, K. & Ellner, J. J. (1999). Drug tolerance in Mycobacterium tuberculosis. *Antimicrob Agents Chemother* **43**, 2600-2606.
4. Wayne, L. G. (1994). Dormancy of Mycobacterium tuberculosis and latency of disease. *Eur J Clin Microbiol Infect Dis* **13**, 908-914.
5. Zhang, Y. (2004). Persistent and dormant tubercle bacilli and latent tuberculosis. *Front Biosci* **9**, 1136-1156.
6. Fenton, M. J. & Vermeulen, M. W. (1996). Immunopathology of tuberculosis: roles of macrophages and monocytes. *Infect Immun* **64**, 683-690.
7. Wayne, L. G. & Hayes, L. G. (1996). An in vitro model for sequential study of shiftdown of Mycobacterium tuberculosis through two stages of nonreplicating persistence. *Infect Immun* **64**, 2062-2069.
8. Betts, J. C., Lukey, P. T., Robb, L. C., McAdam, R. A. & Duncan, K. (2002). Evaluation of a nutrient starvation model of Mycobacterium tuberculosis persistence by gene and protein expression profiling. *Mol Microbiol* **43**, 717-31.
9. Voskuil, M. I., Schnappinger, D., Visconti, K. C., Harrell, M. I., Dolganov, G. M., Sherman, D. R. & Schoolnik, G. K. (2003). Inhibition of respiration by nitric oxide induces a Mycobacterium tuberculosis dormancy program. *J Exp Med* **198**, 705-713.
10. Hu, Y., Mangan, J. A., Dhillon, J., Sole, K. M., Mitchison, D. A., Butcher, P. D. & Coates, A. R. (2000). Detection of mRNA transcripts and active transcription in persistent Mycobacterium tuberculosis induced by exposure to rifampin or

pyrazinamide. *J Bacteriol* **182**, 6358-6365.
11. Schnappinger, D., Ehrt, S., Voskuil, M.I., Liu, Y., Mangan, J.A., Monahan, I.M., Dolganov, G., Efron, B., Butche, P.D., Nathan,C. and Schoolnik, G.K. (2003) Transcriptional Adaptation of Mycobacterium tuberculosis within Macrophages: Insights into the Phagosomal Environment. *J Exp Med*. **198**, 693-704
12. Muttucumaru, N.D.G., Roberts, G. Hinds, J., Stabler, R.A. & Parish, T. (2004) Gene expression profile of Mycobacterium tuberculosis in a non-replicating state. *Tuberculosis* **84**, 239-246
13. Hampshire, T., Soneji, S., Bacon, J., James, B.W., Hinds, J., Laing, K., Stabler, R.A., Marsh, P.D. & Butcher, P.D. (2004) Stationary phase gene expression of Mycobacterium tuberculosis following a progressive nutriuent depletion: a model for persistent organisms? *Tuberculosis* **84**, 228-238
14. Rosenkrands, I., Slayden, R. A., Crawford, J., Aagaard, C., Barry, C. E., 3rd & Andersen, P. (2002). Hypoxic response of Mycobacterium tuberculosis studied by metabolic labeling and proteome analysis of cellular and extracellular proteins. *J Bacteriol* **184**, 3485-3491.
15. Starck, J., Kallenius, G., Marklund, B. I., Andersson, D. I. & Akerlund, T. (2004). Comparative proteome analysis of Mycobacterium tuberculosis grown under aerobic and anaerobic conditions. *Microbiology* **150**, 3821-3829.
16. Cho SH, Goodlett D, & Franzblau, S. (2006) ICAT-based comparative proteomic analysis of non-replicating persistent Mycobacterium tuberculosis. *Tuberculosis* **86**, 445-460.
17. Hutter, B. & Singh, M. (1999). Properties of the 40 kDa antigen of Mycobacterium tuberculosis, a functional L-alanine dehydrogenase. *Biochem J* **343**, 669-672.
18. Hutter, B. & Dick, T. (1998). Increased alanine dehydrogenase activity during dormancy in Mycobacterium smegmatis. *FEMS Microbiol Lett* **167**, 7-11.
19. Worsaae, A., Ljungqvist, L. & Heron, I. (1988). Monoclonal antibodies produced in BALB.B10 mice define new antigenic determinants in culture filtrate preparations of Mycobacterium tuberculosis. *J Clin Microbiol* **26**, 2608-2614.
20. Andersen, A. B., Andersen, P. & Ljungqvist, L. (1992). Structure and function of a 40,000-molecular-weight protein antigen of Mycobacterium tuberculosis. *Infect. Immun.* **60**, 2317-2323.
21. Sawa, Y., Tani, M., Murata, K., Shibata, H. & Ochiai, H. (1994). Purification and characterization of alanine dehydrogenase from a cyanobacterium, Phormidium lapideum. *J Biochem (Tokyo)* **116**, 995-1000.
22. Itoh, N. & Morikawa, R. (1983). Crystallization and properties of L-alanine dehydrogenase from Streptomyces phaeochromogenes. *Agric. Biol. Chem.*, 2511–2519.
23. Yoshida, A. & Freese, E. (1964) Purification and chemical characterization of alanine dehydrogenase from bacillus subtilis. *Biochim Biophys Acta*. **92**, 33-43.
24. Baker, P. J., Sawa, Y., Shibata, H., Sedelnikova, S. E. & Rice, D. W. (1998). Analysis of the structure and substrate binding of Phormidium lapideum alanine dehydrogenase. *Nat Struct Biol* **5**, 561-7.
25. Ohashima, T. & Soda, K. (1979). Purification and properties of alanine dehydrogenase from Bacillus sphaericus. *Eur J Biochem* **100**, 29-30.
26. Grimshaw, C. E. & Cleland, W. W. (1981). Kinetic mechanism of Bacillus subtilis L-alanine dehydrogenase. *Biochemistry* **20**, 5650-5655.
27. Grimshaw, C. E., Cook, P. F. & Cleland, W. W. (1981). Use of isotope effects and pH studies to determine the chemical mechanism of Bacillus subtilis L-alanine dehydrogenase. *Biochemistry* **20**, 5655-5661.

28. Porumb, H., Vancea, D., Muresan, L., Presecan, E., Lascu, I., Petrescu, I., Porumb, T., Pop, R. & Barzu, O. (1987). Structural and catalytic properties of L-alanine dehydrogenase from Bacillus cereus. *J Biol Chem* **262**, 4610-4615.
29. Kutzenko AS, Lamzin VS, & Popov VO. (1998) Conserved supersecondary structural motif in NAD-dependent dehydrogenases. FEBS Lett. 423, 105-109.
30. Qi, G., Lee, R. & Hayward, S. (2005). A comprehensive and non-redundant database of protein domain movements. *Bioinformatics* **21**, 2832-2838.
31. Brändén, C.-I. (1980) Relation between structure and function of α/β proteins. *Quart. Rev. Biophys*. **13**, 317-338
32. Alizade, M. A., Bressler, R. & Brendel, K. (1975). Stereochemistry of the hydrogen transfer to NAD catalyzed by (S) alanine dehydrogenase from Bacillus subtilis. *Biochim Biophys Acta* **397**, 5-8.
33. Stillman, T.J., Baker, P.J., Britton, K.L. & Rice, D.W. (1993) Conformational flexibility in glutamate dehydrogenase. *J. Mol. Biol.* **234**, 1131-1139
34. Cleland, W.W. (1979) Statistical analysis of enzyme kinetic data. *Methods Enzymol.* **63,** 103-138
35. Collaborative Computational Project No. 4 (1994) The CCP4 suite: programs for protein crystallography. *Acta Crystallogr. D*, **50**, 760-763
36. French, S. & Wilson, K. (1978). On the treatment of negative intensity observations. *Acta Cryst. A***34,** 517-525.
37. Rees, D. C. (1980). The influence of twinning by merohedry on intensity statistics. *Acta Cryst. A***36**, 578-581
38. Vagin, A. & Teplyakov, A. (1997). MOLREP: an automated program for molecular replacement. *J. Appl. Crystallogr.* **30**, 1022-1025.
39. Yeates, T. (1997). Detecting and overcoming crystal twinning. *Methods Enzymol.* **276**, 344-358.
40. Storoni, L. C., McCoy, A. J. & Read, R. J. (2004). Likelihood-enhanced fast rotation functions. *Acta Crystallogr D* **60**, 432-438.
41. Brunger, A. T., Adams, P. D., Clore, G. M., DeLano, W. L., Gros, P., Grosse-Kunstleve, R. W., Jiang, J. S., Kuszewski, J., Nilges, M., Pannu, N. S., Read, R. J., Rice, L. M., Simonson, T. & Warren, G. L. (1998). Crystallography & NMR system: A new software suite for macromolecular structure determination. *Acta Crystallogr D* **54**, 905-921.
42. Emsley, P. & Cowtan, K. (2004). Coot: model-building tools for molecular graphics. *Acta Crystallogr D* **60**, 2126-2132.
43. Murshudov, G. N., Vagin, A. A. & Dodson, E. J. (1997). Refinement of macromolecular structures by the maximum-likelihood method. *Acta Crystallogr D* **53**, 240-255.
44. Winn, M. D., Murshudov, G. N. & Papiz, M. Z. (2003). Macromolecular TLS refinement in REFMAC at moderate resolutions. *Methods Enzymol* **374**, 300-21.
45. Laskowski, R. A., MacArthur, M. W., Moss, D. S. & Thornton, J. M. (1993). PROCHECK: A program to check stereochemical quality of protein structures. *J. appl. Crystallogr.* **26,** 283–291.
46. Krissinel, E. & Henrick, K. (2004). Secondary-structure matching (SSM), a new tool for fast protein structure alignment in three dimensions. *Acta Crystallogr D Biol Crystallogr* **60**, 2256-2268.

Table 1: Statistics of data collection and structure refinement. Values in parentheses represent the highest resolution shell.

	ApoAlaDH	***HoloAlaDH***	***AlaDH-NAD+-pyruvate***	***Hybrid hexamer***	***Holo-Asp270Asn AlaDH***
Data collection					
X-ray source	I911.3, MAX-lab	ID23-1, ESRF	ID14.1, ESRF	ID14.1, ESRF	ID14.1, ESRF
Resolution (Å)	2.3 (2.34-2.47)	2.0 (2.04-2.15)	2.0 (2.00-2.11)	2.0 (2.00-2.11)	2.8 (2.8-2.95)
Space group	P321	$P2_13$	$P2_12_12$	$P2_12_12$	$P2_13$
Unit cell a, b, c (Å)	147.1,147.1, 93.7	141.0	176.2,171.8, 98.3	178.9,170.4, 97.8	140.8
no. of subunits in asymmetric unit	2	2	6	6	2
Multiplicity	7.3 (6.1)	6.0 (6.2)	3.2 (2.2)	4.0 (3.9)	4.4 (4.5)
Rsym (%)	7.8 (49.3)	9.7 (57.5)	7.7 (54.0)	9.7 (60.2)	7.5 (40.3)
Mean I/σ (I)	21.1 (2.9)	15.4 (2.8)	10.1 (1.8)	10.1 (2.3)	12.9 (4.1)
Completeness (%)	96.9 (79.2)	99.9 (100)	91.0 (67.2)	99.9 (99.9)	99.0 (99.1)
Wilson B-factor ($Å^2$)	53.9	30.9	27.0	33.2	67.3
No.of reflections overall unique	 345400 (34359) 47413 (5588)	 359770 (52912) 59474 (8596)	 579423 (43130) 182162 (19405)	 811566 (114943) 201126 (29155)	 101582 (14654) 22947 (3294)
Refinement					
Resolution (Å)	45.0 – 2.3	47.7 – 2.04	45.2 – 2.00	20 – 2.00	40.0 - 2.80
Reflection no. Working set Test set	 46272 2332	 59427 2750	 166142 8324	 191428 9572	 21730 1087
R-factor (%) Rfree (%)	21.6* 27.6*	16.4 20.4	16.5 20.4	17.6 21.3	19.4 24.7
B-factor ($Å^2$) protein atoms ligands water molecules	 46.8 31.3	 33.8 27.5 (NADH) 40.1	 21.8 15.1 (NAD+) 42.1(pyruvate) 28.8	 44.8 33.4 (NADH) 51.2	 46.8 40.8 (NADH) 43.3
R.m.s.d Bond distance Bond angle	 0.008 1.40	 0.013 1.46	 0.015 1.61	 0.013 1.51	 0.011 1.41
Ramachandran plot: residues in most favorable additionally allowed disallowed regions (%)	 84.7 15.1 0.2 0	 93.8 5.9 0.3 0	 93.0 6.7 0.3 0	 93.5 6.2 0.3 0	 90.6 8.9 0.5 0

*: twinned R-values calculated in CNS.

Table 2: Kinetic parameters of wild-type and mutant *Mt*AlaDH for L-alanine and pyruvate.

Enzyme	oxidative deamination		reductive amination	
	k_{cat} (sec^{-1})	K_m L-alanine (mM)	k_{cat} (sec^{-1})	K_m pyuvate (mM)
Wild-type	126±4	15.64±1.09	694±33	0.76±0.05
H96A		inactive		inactive
D270A		inactive		inactive
D270N		inactive		inactive

Figure legends

Figure 1: Proposed catalytic steps for the conversion of pyruvate and ammonia to L-alanine, catalyzed by AlaDH, adapted from[27]. X and Y are two groups on the enzyme that may act as acid/base catalysts. The identity of these groups is discussed in the text. It is likely that the attack of ammonia occurs from the opposite side of the substrate than the attack of the water molecule in the reverse reaction. The stereochemistry of the carbinolamine intermediate is not yet resolved, and the approach of ammonia can therefore in principle occur from above the plane of the paper (as drawn here) or below the plane of the paper. The nicotinamide ring is below the substrate, and hydride transfer results in the formation of L-alanine.

Figure 2: Molecular architecture of L-AlaDH from *Mycobacterium tuberculosis*. A. Schematic cartoon of the structure of the enzyme subunit in the closed conformation. The bound cofactor NAD+ and pyruvate are shown as ball-and-stick models. B. Cα trace of the dimer of *Mt*AlaDH. One subunit is shown in blue (NAD binding domain) and red (substrate binding domain), and the second subunit is shown in grey. The positions of the active sites are highlighted by the bound ligand NAD+. Note that the dimer interface is opposite to the active sites, rendering them accessible to substrate. C. The hexameric AlaDH molecule of *Mycobacterium tuberculosis*. upper panel: view along the molecular three-fold axis, indicated by a triangle. Lower panel: side view of the hexamer, with the three-fold axis in the plane of the paper. The NAD domains are shown in blue, and the substrate binding domains in red.

Figure 3. NADH binding to *Mt*AlaDH. A. Change in fluorescence emission (arbitrary units) at 390 nm as a function of NADH concentration. Experimental data points are indicated by dots, and the line represents the fit of the following equation[34] to these data points: $\Delta A_{390}=\Delta A_{390,\ max}$ (NADH)/(K_d + (NADH)). B. Plot of initial rates of reductive amidation as a function of NADH concentration in 100 mM NH_4Cl/NH_3 buffer at pH 7.4. The concentration of pyruvate was 20 mM C. Stereoview of the surroundings of bound NADH in *Mt*AlaDH. Dotted lines indicate hydrogen bonds (distance < 3.2 Å). The 2Fo-Fc electron density map is contoured at 1.0σ. Underlined labels indicate conserved residues.

Figure 4: Stereoview of an overlay of the Cα traces of apo- (blue) and holo- (green) *Mt*AlaDH. The superposition is based on a structural alignment of the NAD domains. The co-enzyme NADH (red) is shown as stick model.

Figure 5: Ternary complex of *Mt*AlaDH with NAD+ and formate/pyruvate. A. Part of the refined 2Fo-Fc electron density map, shown in blue, at the active site of the ternary complex, illustrating that a model of formate alone does not account for the difference electron density. The Fo-Fc electron density map obtained after refinement of the *Mt*AlaDH/NAD+/formate complex is contoured in green at +3.0 σ, showing significant residual electron density close to the formate ion. B. Part of a composite omit map of the refined ternary complex of *Mt*AlaDH with pyruvate and NAD+, showing that the pyruvate molecule is not bound with full occupancy. The electron density map is contoured at 1.0σ.

Figure 6: Stereoview of the active site in the ternary complex of *Pl*AlaDH with pyruvate and NAD+. For better clarity, only parts of NAD+ are showen (Ad, adenine ribose). The structure of *Pl*AlaDH (PDB code 1say) in complex with pyruvate (green carbon bonds) is superimposed on the NAD domain of *Mt*AlaDH (blue carbon bonds). Black labels denote residues from *Pl*AlaDH, and red labels residues from *Mt*AlaDH.

Figure 7: Gatekeeper role of Lys75 in MtAlaDH. A. Surface representation of the enzyme in the vicinity of the active site. The pyruvate molecule is inaccessible to solvent, including the substrates water and ammonia. B. Changes in solvent accessibility resulting from the proposed conformational change of the side chain of Lys75. The channel leading from the enzyme surface to the *si* face of pyruvate is clearly visible. Solvent accessibilities of carbon, nitrogen, and oxygen atoms are shown in gray, blue, and red colours, respectively.

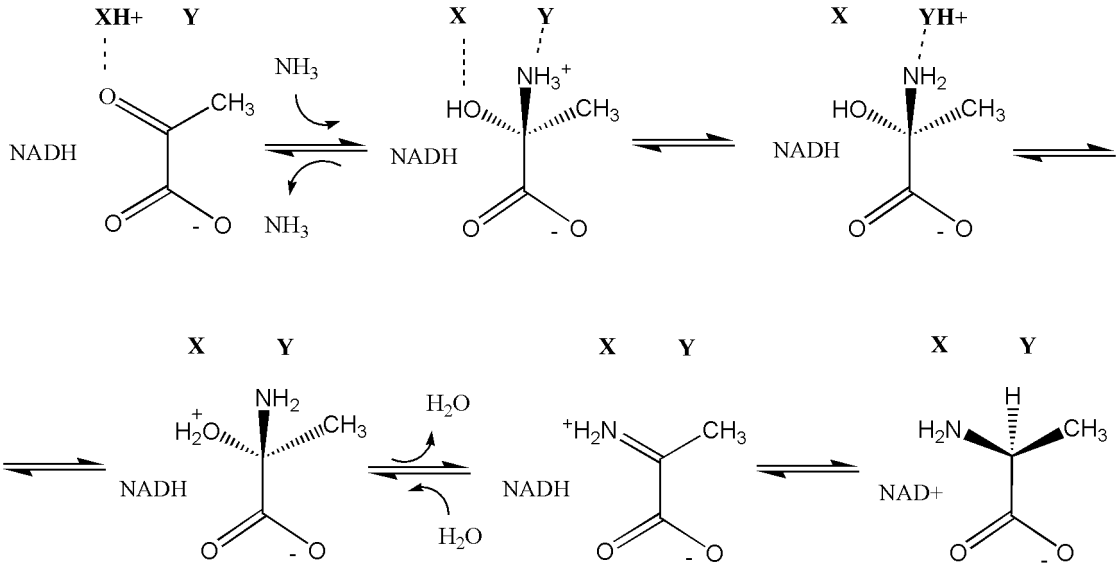

Figure 1

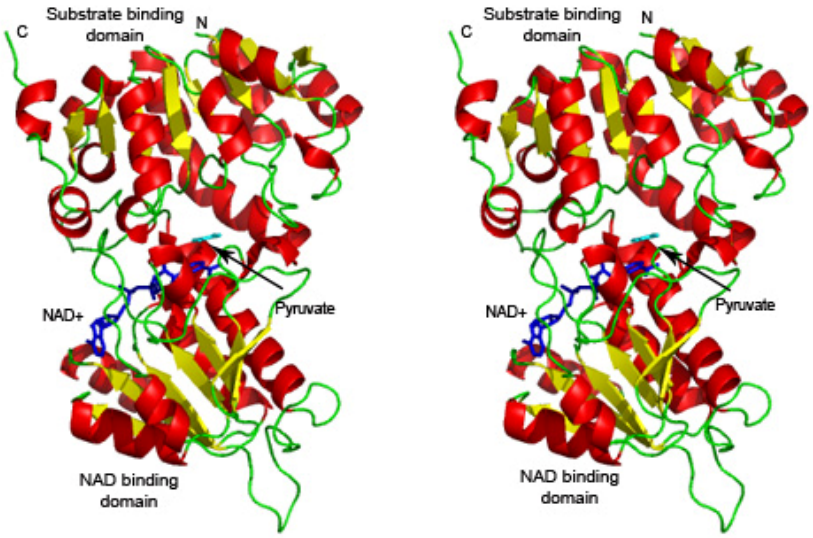

Figure 2a (stereo, double column)

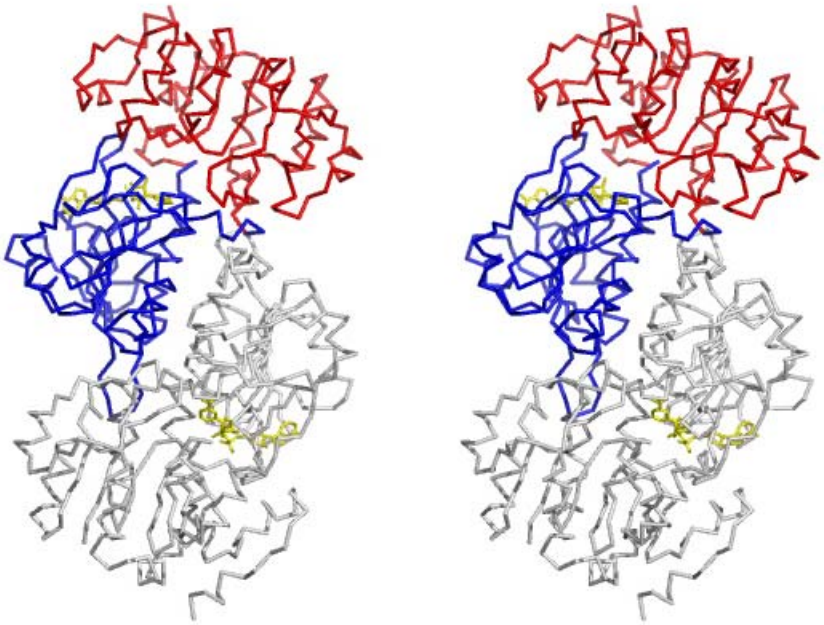

Figure 2b (stereo, double column)

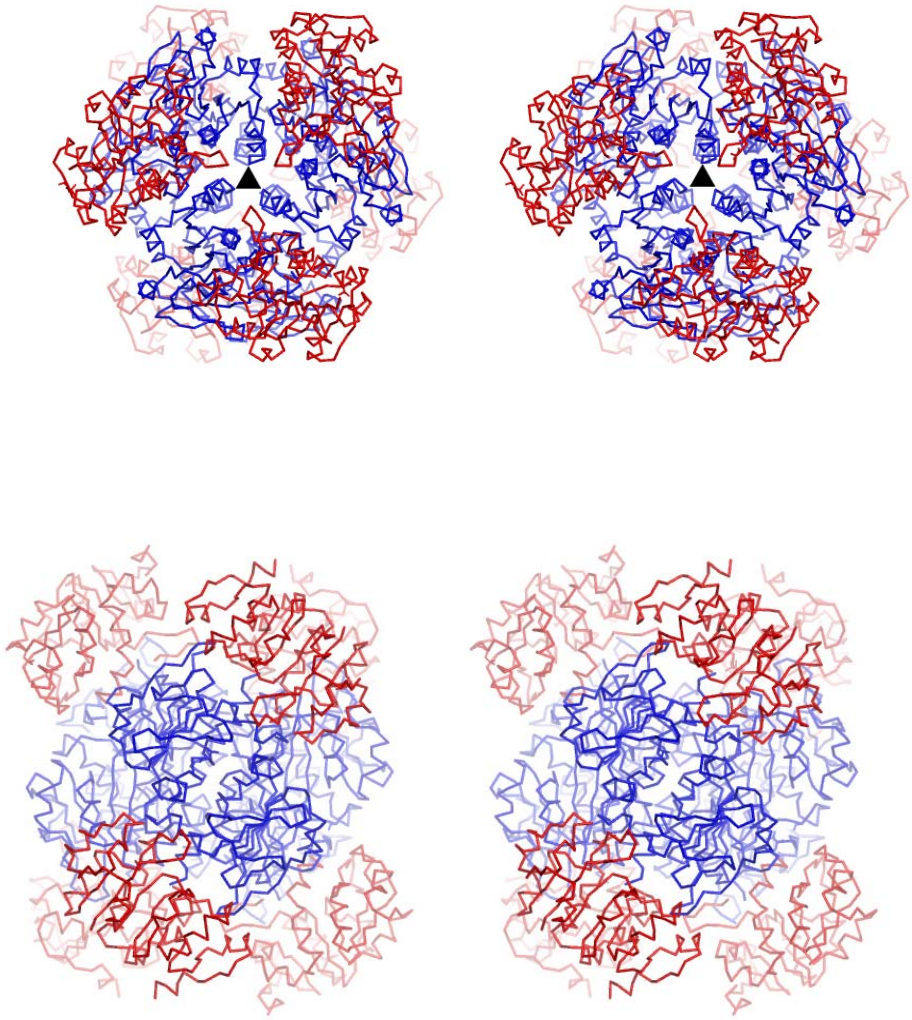

Figure 2c (stereo, double column)

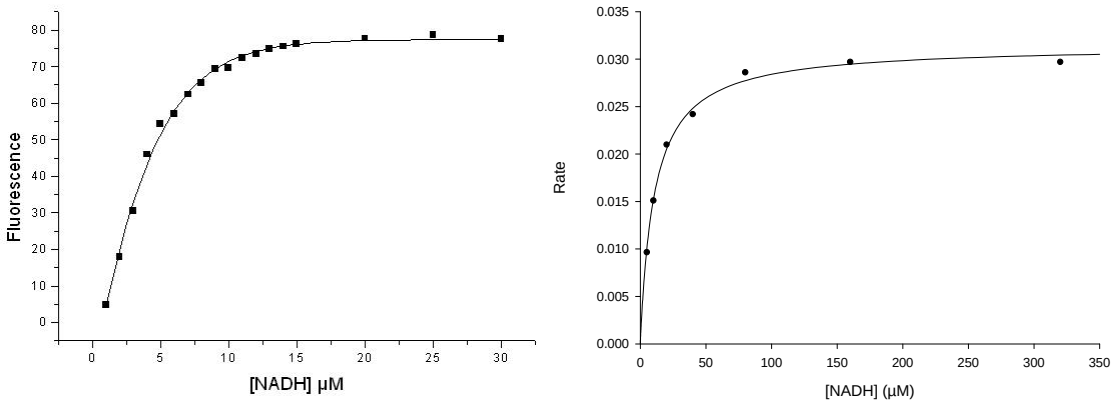

Figure 3a (left) and 3b (right) (double column)

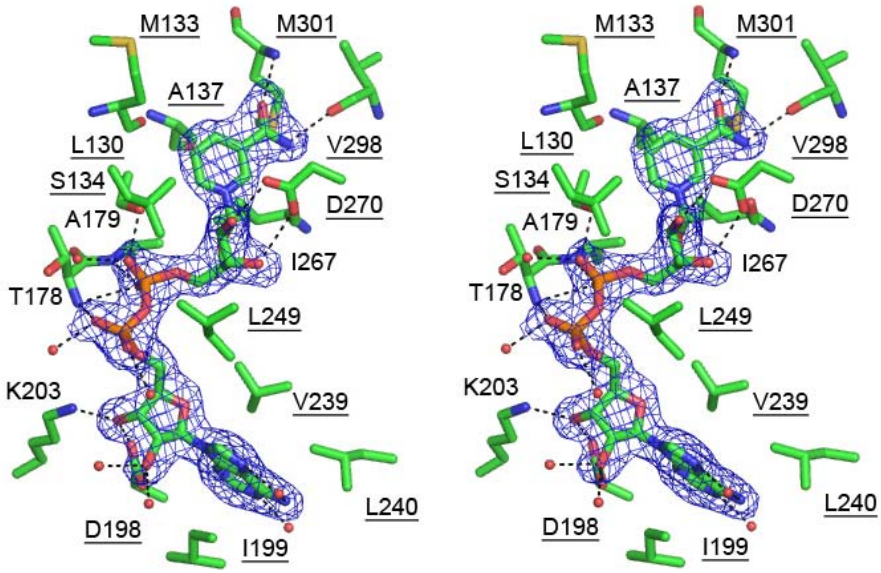

Fig 3c (stereo, double column)

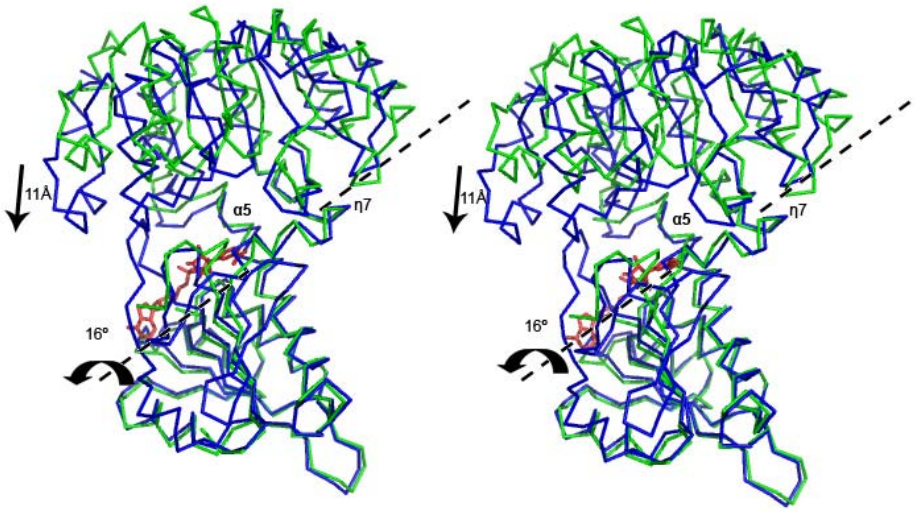

Fig 4 (stereo, double column)

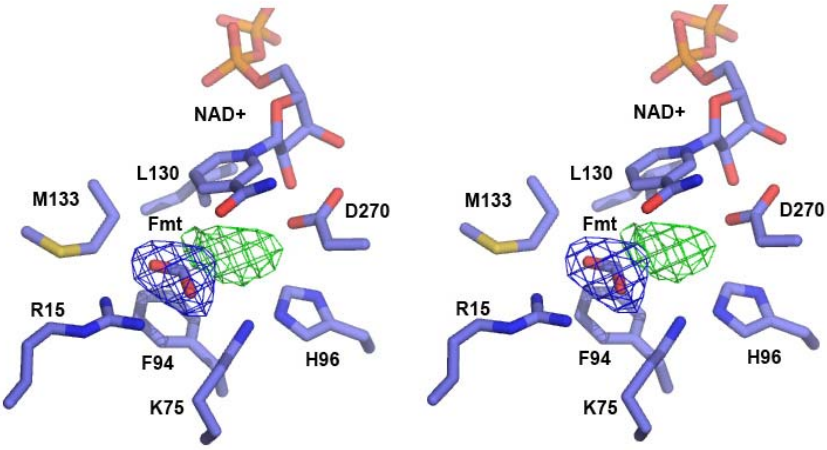

Figure 5a (stereo, double column)

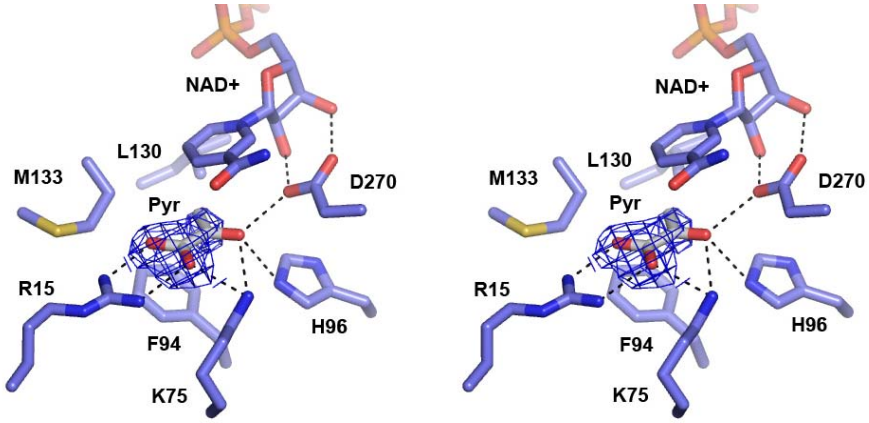

Figure 5b (stereo, double column)

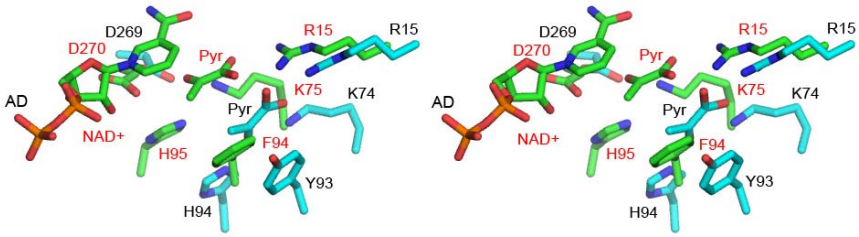

Figure 6 (stereo, double column)

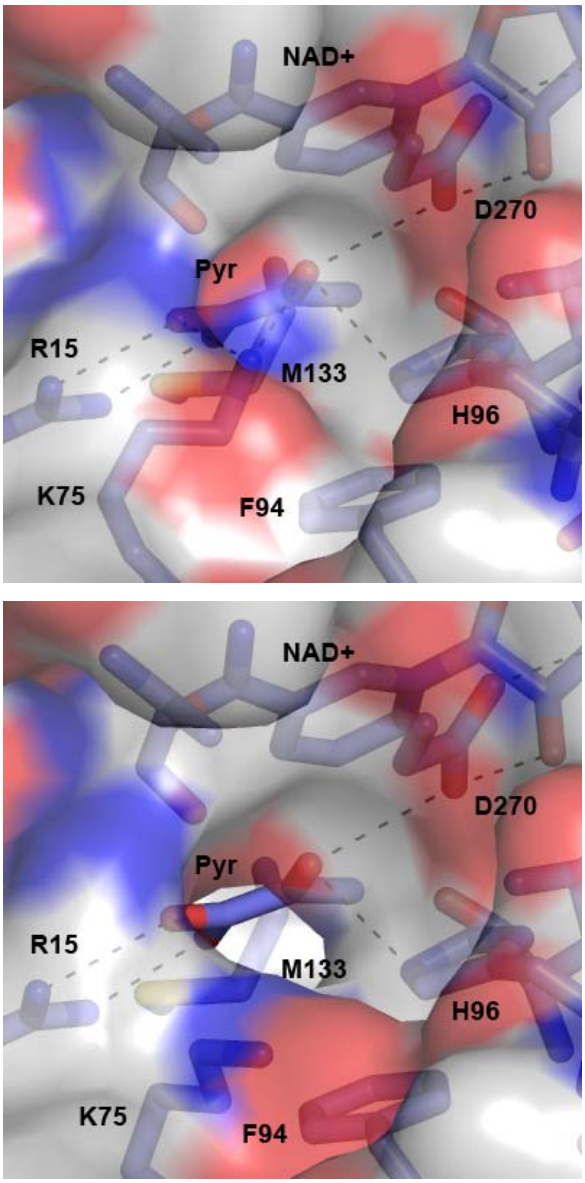

Figure 7 (single column)